

1 This document is the Submitted Manuscript version of a Published article
2 that appeared in final form in the *Drug Delivery and Translational Research*, copyright SPRINGER.
3 To access the final edited and published work see: <https://doi.org/10.1007/s13346-023-01302-1>

4 5 Development of a 3D printed *in vitro* integrated oro- 6 pharyngeal air-liquid interface cellular throat model for 7 drug transport

8
9 Zara Sheikh^{1,7*}, Antonella Granata^{1*}, Ye Zhang^{1,3}, Hanieh Mohammad Gholizadeh
10 Mahvizani¹, Dina Silva^{1,4}, Paul M Young^{1,5}, Luca Casettari⁶, Hui Xin Ong^{1,2 *}, Daniela
11 Traini^{1,2*}

12
13 ¹Respiratory Technology, The Woolcock Institute of Medical Research, Glebe, NSW 2031,
14 Australia

15 ²Faculty of Medicine, Health and Human Sciences, Macquarie Medical School, Macquarie
16 University, Sydney, NSW 2109, Australia

17 ³School of Mechanical Engineering, Faculty of Engineering, Macquarie University, Sydney,
18 NSW 2109, Australia

19 ⁴Ab-intio Pharma, NSW 2050, Australia

20 ⁵Macquarie Business School, Macquarie University, Sydney, NSW 2109, Australia

21 ⁶University of Urbino Carlo Bo, Department of Biomolecular Sciences, Urbino, Italy

22 ⁷School of Pharmacy, Brac University, Dhaka, Bangladesh

23 24 25 26 27 28 29 30 31 32 33 34 35 **Correspondence:**

36 Zara Sheikh

37 Email: zara.sheikh@sydney.edu.au

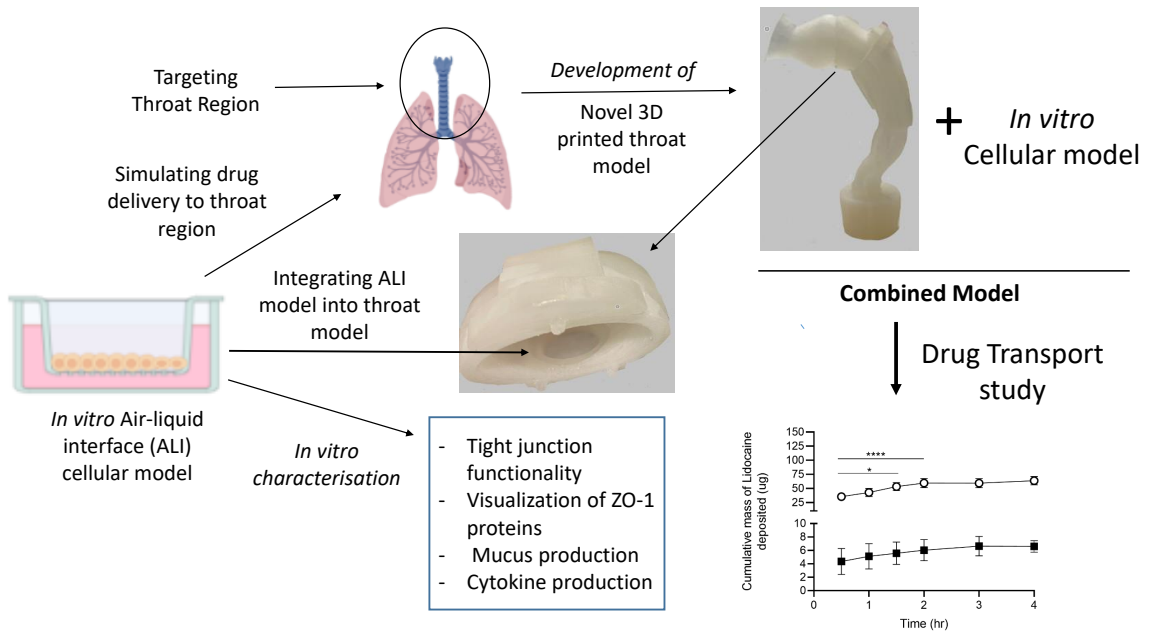
40 **ABSTRACT**

41 To simulate the deposition of drugs in the oro-pharynx region, several *in vitro* models are
42 available such as the United States Pharmacopeia-Induction Port (USP-IP) throat and the
43 Virginia Commonwealth University (VCU) models. However, currently, there is no such *in*
44 *vitro* model that incorporates a biological barrier to elucidate drug transport across the
45 pharyngeal cells. Cellular models such as *in vitro* air-liquid interface (ALI) models of human
46 respiratory epithelial cell lines are extensively used to study drug transport. To date, no studies
47 have yet been performed to optimise the ALI culture conditions of the human pharyngeal cell
48 line Detroit 562 and determine whether it could be used for drug transport. Therefore, this study
49 aimed to develop a novel 3-D printed throat model integrated with an ALI cellular model of
50 Detroit 562 cells and optimise the culture conditions to investigate whether the combined
51 model could be used to study drug transport, using Lidocaine as a model drug. Differentiating
52 characteristics specific to airway epithelia were assessed using 3 seeding densities (30,000,
53 60,000, and 80,000 cells/well (c/w), respectively) over 21 days. The results showed that Detroit
54 562 cells completely differentiates on day 18 of ALI for both 60,000 and 80,000 c/w with
55 significant mucus production, showing response to bacterial and viral stimuli and development
56 of functional tight junctions and Lidocaine transport with no significant differences observed
57 between the ALI models with the 2 cell seeding densities. Results showed the suitability of the
58 Low density (60,000 c/w or 1.8×10^5 cells/cm²) ALI model to study drug transport.
59 Importantly, the developed novel 3-D printed throat model integrated with our optimised *in*
60 *vitro* Detroit 562 ALI model showed transport of Lidocaine throat spray. Overall, the study
61 highlights the potential of the novel 3-D printed bio-throat integrated model as a promising *in*
62 *vitro* system to investigate the transport of inhalable drug therapies targeted at the oro-
63 pharyngeal region.

64 **Keywords:** *in vitro* throat model, Detroit 562, air-liquid interface, paracellular transport,
65 Lidocaine, 3D printing.

66 **GRAPHICAL ABSTRACT**

67
68



69
70
71
72
73
74
75
76
77
78
79
80
81
82
83
84
85
86

87 **1. INTRODUCTION**

88 The airway epithelium lining the respiratory tract is a continuous cellular layer of different cell
89 types, starting from the nasopharynx to the alveoli, forming a protective barrier between the
90 inhaled air and the underlying mucosal tissue [1]. Drugs and toxins must cross this barrier to
91 reach their target site and elicit a therapeutic or noxious effect. *In vitro* air-liquid interface
92 (ALI) of human respiratory epithelial cell lines is an invaluable tool that phenotypically mimics
93 the *in vivo* airway epithelium, extensively used to study drug transport, and evaluate the fate of
94 inhaled drugs and toxins. These models can be used to predict immune responses and
95 therapeutic efficacy owing to their ease of culture, genetic homogeneity, and greater
96 reproducibility [2, 3]. These *in vitro* ALI models are established when cells are seeded on the
97 apical side of a semi-permeable support membrane, allowing nutrients from the basal media to
98 pass through the membrane. Upon reaching confluency, the culture medium from the apical
99 layer is removed, enabling cell growth and differentiation on the apical, air-exposed surface [4,
100 5]. Thus, cells grown in ALI conditions undergo differentiation and polarization, forming
101 junctional complexes that recapitulate the key *in vivo*-molecular and structural characteristics
102 of the cells present in the airway epithelium [6].

103 The ability of the cells to form polarised layers of confluent cells and consequently the
104 ‘tightness’ of the epithelium is one of the key parameters that determine the suitability of an *in*
105 *vitro* cell model to be used for drug transport and other biopharmaceutical studies [7]. Polarized
106 epithelial cells are connected via junctional complexes comprising of tight junctions and
107 adheren junctions that enable cell-cell adhesion and barrier integrity [8]. These tight junctions
108 form a paracellular barrier that permits the movement of ions and small molecules across the
109 airway epithelium, thus limiting the paracellular transport of drugs [9, 10].

110 Currently, there are several therapies including local anaesthetics, antibiotics and mucolytic
111 agents that are targeted at the oro-pharyngeal region for various therapeutic and prophylactic

112 purposes. However, there is a lack of an established model that could be used to study these
113 therapies targeted at the oro-pharyngeal region. Lidocaine, a local anaesthetic used before
114 surgical interventions, is commercially available as a throat spray. As the Detroit 562 cell line
115 represents the pharynx, these cells could be utilized to investigate the deposition of such
116 therapies targeted in the oropharyngeal region to understand the therapeutic activity.

117 Several studies have utilized the human pharyngeal cell line Detroit 562 under ALI and in
118 liquid-covered cultures to investigate immune responses to bacterial colonisation and innate
119 signalling and regulatory pathways [11-13]. However, to date, no studies have been performed
120 to systematically characterise and optimise the ALI culture condition (seeding density and
121 culture time) of the Detroit 562 cell line and further determine whether these ALI models could
122 be used to study drug transport.

123 Realistic physical mouth-throat (MT) models have been developed to predict the *in vivo* drug
124 deposition in the oro-pharyngeal region for drug product development and bioequivalence
125 assessment of inhalation drug products [14]. The USP induction port simulating the MT region
126 is the recommended attachment for impaction studies to determine drug deposition patterns by
127 the United States Pharmacopeia. However, as the USP port is a metallic tube with a 90° bend,
128 the design of the port does not include the special geometrical features that are fundamental to
129 accurately predicting the *in vivo* drug deposition in the throat region. Consequently, several
130 MT models have been developed to address this issue [15-18]. Among these models, the MT
131 models developed by Byron's group at Virginia Commonwealth University (VCU), widely
132 known as the VCU models, have shown enhanced *in vitro-in vivo correlation* for several
133 marketed inhalation products compared to the other MT models [19-21].

134 Currently, there are no mouth-throat models that incorporate an *in vitro* cellular model to study
135 the deposition of aerosol drugs targeted at the oro-pharyngeal region and in turn drug transport

136 across the epithelial layers of the pharyngeal cells for greater physiological relevance.
137 Furthermore, there is no consensus or guidelines for the flow rate or spray angle used for testing
138 such throat spray formulations using the available compendial models. Therefore, our study
139 first aims to determine the appropriate culture method required to develop tight junctions and
140 establish the epithelial barrier properties of the *in vitro* ALI model of the Detroit 562 cell line
141 and to further investigate whether the developed model could be used to study drug transport,
142 using Lidocaine as a model drug. Next, we focused on modifying the current medium-sized
143 VCU throat model by introducing the novel concept of incorporating pharyngeal cells (Detroit
144 562 ALI model) within the model. The overall aim of the study is to develop an *in vitro* throat
145 model incorporating a cellular model representative of the oropharyngeal region to investigate
146 drug deposition and transport of throat sprays across the cellular layers, using Lidocaine throat
147 spray as a model drug. This will be accompanied by studying the impact of flow rates and spray
148 angle on aerosol deposition in the oropharyngeal region for the testing of such formulations.

149 **2. MATERIALS AND METHODS**

150 **2.1 Materials**

151 Lidocaine base, sodium fluorescein (flu-Na), Hanks' Balanced Salt Solution (HBSS), were
152 purchased from Sigma Aldrich (Sydney, Australia). Ethanol (100 %) and acetonitrile were
153 purchased from Chem-Supply Pty Ltd (Australia) and PTFE 0.45 µm filter was purchased from
154 FilterBio® (China). All cell culture reagents including Dulbecco's modified eagle's medium
155 (DMEM), Minimum Essential Medium Eagle (MEM), phosphate-buffered saline (PBS), foetal
156 bovine serum (FBS), trypsin-EDTA solution (2.5 g/l trypsin, 0.5 g/l EDTA), L-glutamine
157 solution, non-essential amino acids were obtained from Invitrogen (Sydney, Australia). Water
158 was purified by reverse osmosis (MilliQ, Millipore, France). All solvents used were of
159 analytical grade.

160 **2.2 Cell lines**

161 Detroit 562 (Immortalised Epithelial Human Pharyngeal cells- carcinoma derived) were
162 purchased from the American Type Culture Collection (VA, USA). All cells were maintained
163 in minimum essential cell growth medium (MEM)) supplemented with FBS (10 %) and L-
164 glutamine (1 %) and incubated at 37 °C under 5 % CO₂. All experiments were conducted
165 between passage numbers 51- 62 for the Detroit 562 cell line.

166 **2.3 Air-Liquid Interface (ALI) culture of Detroit 562 cells**

167 To establish an *in vitro* ALI model of Detroit 562 cells, Transwell cell culture inserts (0.33
168 cm², polyester terephthalate (PET) membrane, 0.4 µm pore size) (Corning Costar, USA) were
169 used as previously described [22]. To determine the appropriate seeding density for Detroit 562
170 cell line, three different seeding densities were chosen: 30,000 cells/well (c/w) (0.9×10^5
171 cells/cm²), 60,000 c/w (1.8×10^5 cells/cm²) and 80,000 c/w (2.4×10^5 cells/cm²). Briefly,
172 Detroit 562 cells were seeded within the apical chamber in MEM media supplemented with
173 10% v/v FBS and 1% L-glutamine and the same media was added to the basolateral chamber.
174 The cells were incubated at 37°C with 5% CO₂ for 24 hours until confluency was achieved. To
175 initiate ALI conditions, media in the apical chamber was removed after 24 hours indicating day
176 0 and the cells were maintained under ALI conditions for 21 days. Differentiation media in the
177 basolateral chamber was replaced every 2 days. All experiments were performed on day 7, 14,
178 18 and 21 post ALI induction.

179

180 **2.4 Transepithelial Electrical Resistance (TEER)**

181 Transepithelial electrical resistance (TEER) was measured as described previously. Briefly,
182 pre-warmed media was added to the apical chamber and allowed to equilibrate for 30 mins at
183 37 °C under 5 % CO₂. TEER was measured using EVOM2[®] epithelial voltohmmeter (World

184 Precision Instruments, USA) attached to STX-2 chopstick electrodes for the ALI cultures,
185 corrected by subtracting the blank inserts, and multiplied by the area of the Transwell inserts
186 (0.33 cm²) and six measurements were taken per Transwell.

187

188 **2.5 Sodium fluorescein permeability assay**

189 Tight junction functionality and paracellular permeability of Detroit 562 ALI cultures were
190 determined using the sodium fluorescein permeability assay. Sodium fluorescein (2.5 mg/mL),
191 (Sigma Aldrich, Sydney, Australia) was added to the apical chamber and pre-warmed Hanks'
192 Balanced Salt Solution (HBSS) was added to the basolateral chamber. Transwells were
193 incubated for 4 hours at 37 °C with 5 % CO₂, with basolateral samples (100 µL) collected and
194 replaced with fresh HBSS after every 30 minutes for the first 2 hours and then every hour for
195 the final 2 hours to measure the rate of transport (flux) of the sodium fluorescein from the apical
196 chamber to the basolateral chamber. For analysis, the collected basolateral samples were
197 diluted (1:20) and fluorescence was measured using the SpectraMax M2 plate reader
198 (excitation: 485 nm; emission: 538 nm). The permeation coefficient (P_{app}) was calculated
199 according to equation 1.

200 Eq 1.
$$P_{app} = \frac{dQ}{dT \cdot C_0 \cdot A}$$

201 where dQ/dT represents the flux of sodium fluorescein (µg/s) across the membrane, C₀ is the
202 initial donor concentration (µg/mL), and A is the surface area (cm²).

203

204 **2.6 Live and Dead Cell Staining**

205 LIVE/DEAD[®] Viability/Cytotoxicity Kit (Molecular Probes) and the Hoechst stain (Sigma
206 Aldrich) were used to stain the ALI cultured cell layers. The assay was performed as per the

207 manufacturer's instructions. Briefly, the cell layer was washed 3 times with pre-warmed PBS
208 and 2 μ M calcein AM and 4 μ M ethidium homodimer-1 (EthD-1) were added to the apical
209 compartment. Cells were incubated with the solution for 30 minutes in the dark at room
210 temperature. Cells were incubated with Hoechst (1:10000) for 10 minutes to stain the nucleus.
211 The Transwell membranes containing the cell layer were excised and mounted on a glass
212 microscope slide for analysis. Cells were imaged using a Nikon ECLIPSE Ti inverted
213 microscope controlled by the NIS Elements software (Nikon) and equipped with the APO Fluor
214 20X air objective. Images were captured using a CoolSNAP ES2 high-resolution digital camera
215 (Photometrics). 10 images of different fields of view were taken per Transwell membrane.

216

217 **2.7 Mucus production**

218 Mucus production of the ALI cultures was characterized by staining the glycoproteins (mucins)
219 with alcian blue as previously described. Briefly, cell layers were washed twice with
220 prewarmed PBS and fixed using 4% paraformaldehyde (v/v) for 15 minutes. Subsequently, the
221 cells were washed thrice with PBS and Alcian blue (1% w/v Alcian blue in 3% v/v acetic
222 acid/water at pH 2.5) was added to the apical chamber and incubated for 20 minutes. The cell
223 layer was washed up to 10 times with PBS to remove excess Alcian blue and allowed to air-
224 dry for 3 hours at room temperature. The Transwell membranes containing the cell layer were
225 excised and mounted on a glass microscope slide for analysis. Mucus staining was imaged
226 using an Olympus BX61 microscope (Olympus) equipped with an Olympus DP71 camera and
227 a 20X air objective. 10 different fields of view were captured per Transwell membrane. Images
228 were analyzed using Image J software (NIH).

229 **2.8 Evaluation of cytokine production and inflammatory responses**

230 Lipopolysaccharide (LPS) from *E.coli* (Sigma-Aldrich) was resuspended at 10 μ g/mL in
231 differentiation media (MEM with 10 % FBS and 1% L-glutamine) and added to the basolateral

232 chamber to stimulate the cells to model bacterial infection. The cells were stimulated with
233 polyinosinic-polycytidylic acid (Poly (I:C)) (10 µg/mL, Sigma Aldrich) by resuspending in the
234 differentiation media to model viral infection. Cells were then incubated at 37 °C under 5 %
235 CO₂ for 24 and 48 hours and untreated cells served as the control. After treatment, samples
236 were collected from the basolateral culture medium for subsequent analysis of IL-6, IL-8 and
237 IL-1β cytokine production using an enzyme-linked immunosorbent assay (ELISA) kit (BD
238 OptEIA, BD Biosciences) according to the manufacturer's instructions.

239 **2.9 Immunofluorescence**

240 The presence of tight junctions in the ALI cultures was visualized by immunolabeling tight
241 junction proteins Zonula Occludens-1 (ZO-1). Cell layers were washed 3 times with PBS and
242 fixed with 4 % paraformaldehyde (v/v) for 15 min. The cell layers were then washed 3 times
243 with PBS and permeabilised following a 10 min incubation with 0.2 % Triton X-100 (v/v) and
244 then blocked and quenched with 10% normal goat serum (v/v) (Invitrogen) and 0.3 M glycine
245 (Sigma Aldrich) respectively, and incubated for 1 h at room temperature. The primary
246 antibody, ZO-1 rabbit polyclonal (Abcam) (1:200) was incubated overnight at 4 °C. The next
247 day, the cell layers were washed 3 times with PBS and incubated with goat anti-rabbit Alexa
248 Fluor[®] 488 (Life Technologies) (1:500) for 2 h at room temperature. Cell layers were then
249 counterstained with DAPI (Sigma Aldrich) (1:10000) and incubated for 30 min at room
250 temperature. Finally, Transwell membranes containing the cell layer were excised and mounted
251 using FluoroSave mounting media (Millipore) on a glass microscope slide for analysis.

252 Cells were imaged using a confocal microscope (Nikon Eclipse Ti) equipped with a Plan Apo
253 VC 60 × oil objective. Images were taken using the resonant scanner at a step size of 0.31 µm,
254 512 × 512 pixels with an average line scan of 16. For cells immunolabelled with FITC-tagged
255 secondary antibodies, the 488 nm laser was set to 3.5 % with a smart gain of 55 V and an offset

256 of -3 %. For nuclei excitation, the 405 nm laser was again set to 3 % with the smart gain and
257 offset set to 50 V and -1 % respectively.

258

259 **2.10 Lidocaine transport study**

260 To investigate whether the developed ALI model of the Detroit 562 cell line could be used to
261 study drug transport, a study was conducted using Lidocaine as a model drug. Lidocaine
262 transport across the Detroit 562 ALI cultures was conducted on day 18 post ALI formation.
263 Lidocaine was dissolved in ethanol to produce the stock solution and then further diluted in
264 HBSS to prepare a 20 µg/mL Lidocaine (0.1 % ethanol in final Lidocaine solution) to be used
265 for the transport study. Lidocaine solution was added to the apical chamber and HBSS was
266 added to the basolateral chamber. Samples (100 µL) were taken from the basolateral chamber
267 every 30 min for the first 2 h and then every hour for the final 2 h, with samples being replaced
268 by fresh, warm HBSS. After the 4 h assay, the apical chamber was washed twice with HBSS
269 to collect any residual drug using a pipette (denoted as On) and the cell layer was then scraped
270 from the insert membrane and lysed using CelLytic™ buffer (Invitrogen) to quantify the
271 amount of drug inside the cells (denoted as Cellular). TEER measurements were performed
272 before and after the transport, study to check whether drug deposition altered the epithelial
273 barrier integrity of Detroit 562 ALI culture models. All the samples were subsequently
274 analysed using High-Performance Liquid Chromatography (HPLC) using the quantification
275 method described in the next section.

276 **2.11 HPLC quantification method for Lidocaine**

277

278 All Lidocaine samples were analysed using a High-Performance Liquid Chromatography
279 (HPLC) system equipped with SPD-20A UV-Vis detector, an LC-20AT liquid chromatograph,
280 a SIL-20A HT autosampler (Shimadzu) and a Kinetex C-18 column (250 × 4.6 mm, 5 µm,
281 Phenomenex, Torrance, USA), according to a validated method. The mobile phase was a

282 mixture of acetonitrile: phosphate buffer (26:74 (v/v) with pH 5.5 adjusted using sodium
283 hydroxide (Sigma Aldrich). Samples were analysed at 230 nm at a flow rate of 1.0 mL/minute
284 and an injection volume of 10 μ L. Linearity was obtained between 0.2 and 100 μ g/mL ($R^2 =$
285 0.99) with a retention time of 8 min.

286

287 **2.12 Development of a 3D printed throat model incorporated with cells**

288 To evaluate drug deposition and transport of inhaled drugs targeted at the oropharyngeal
289 region, a realistic and more physiologically relevant throat model was designed and developed
290 to include the integration of cells for enhanced *in vitro-in vivo* correlation. A computer-aided
291 (CAD) design of the medium-sized Virginia Commonwealth University (VCU) throat model
292 was prepared by AutoCAD[®] (version 23, USA). The design was modified to connect two
293 separate lower and upper pieces and insertion of two Snapwell inserts (denoted as Upper and
294 Lower snapwells respectively) in which cells grown in ALI conditions could be incorporated
295 for subsequent deposition and transport studies (Figure 1). The prepared 3D design was then
296 3D printed using clear photopolymer resin (FLGPCL02, Formlabs Inc., USA) by
297 stereolithography (SLA), using Form 2 (Formlabs Inc., USA).

298

299 **2.13 *In vitro* aerosol deposition using USP-IP and the 3D printed throat models**

300 Deposition profiles of the Lidocaine spray targeted to the throat were determined using the
301 European Pharmacopeia Apparatus E, Next Generation Impactor (NGI) (Copley Instruments
302 Ltd) fitted with the USP stainless steel 90° induction port (US-IP model), as specified in
303 European Pharmacopoeia (Ph. Eur. 8th Edition, monograph 2.9.18). To optimise the conditions
304 for studying the throat deposition of Lidocaine spray, the experiment was performed at two
305 different angles of spraying (45° and 90°) with 3 different flow rates of 0, 15 and 30 L/min
306 representing no airflow, light breathing and normal breathing condition respectively. Briefly,
307 the NGI was connected to a high-capacity vacuum pump, and the flow rate was set using a flow

308 meter (Model 4040, TSI Precision Measurement instruments). Lidocaine throat spray was
309 primed by firing 5 shots to waste and weighed before each shot. The distance between the spray
310 nozzle and the throat was measured at 7 cm for each NGI experiment to ensure that the spray
311 is aimed primarily toward the throat and not in the oral cavity. The Lidocaine throat spray was
312 attached to the impactor via an airtight adaptor with an actuation time of 4 s. Following the
313 completion of the delivered dose, all components of the NGI (actuator, adaptor, IP, stages 1–7
314 and micro-orifice collector (MOC)) were washed with acetonitrile: phosphate buffer (26:74
315 (v/v), transferred to volumetric flasks and sonicated for 10 mins. Samples were then filtered
316 (0.45 μm , PTFE) and Lidocaine was quantified using HPLC. Subsequently, the flow rate that
317 resulted in maximum Lidocaine deposition in the throat region was used to determine drug
318 deposition using our novel 3-D printed VCU model at both 45 and 90° angles. All the samples
319 were subsequently analysed using a High-Performance Liquid Chromatography (HPLC)
320 quantification method for Lidocaine described in the previous section.

321

322 **2.14 Transport of Lidocaine throat spray using the 3D printed VCU model** 323 **integrated with Detroit 562 ALI culture**

324

325 To investigate whether the developed novel 3D printed VCU model integrated with the ALI
326 model of Detroit 562 cells grown on Snapwells could be used to study drug transport of
327 Lidocaine throat spray, a transport experiment was conducted over a 4-h period. Prior to
328 conducting the transport study, optimization of the number of shots of the throat spray on the
329 cellular layers of the Detroit 562 ALI culture was performed at the optimised flow rate of
330 30L/min and an angle of 45° using 1 shot and 3 shots of Lidocaine spray. Using the optimised
331 conditions, deposition, and transport of lidocaine spray across the Detroit 562 cells grown in
332 ALI conditions on snapwell inserts placed within the 3D-printed VCU throat model were
333 studied. The snapwells with the Detroit 562 cells were placed in the lower and upper part of

334 the 3D throat model and hence referred to as Lower and Upper snapwells respectively.
335 Lidocaine throat spray was attached to the impactor via an airtight adaptor and one shot was
336 fired into the 3D throat at an angle of 45°. After deposition, the snapwell inserts were removed
337 from the 3D printed throat and transferred into culture plates with 2 mL of fresh HBSS added
338 into the basal chamber. Samples (200 µL) were taken from the basolateral chamber every 30
339 min for the first 2 h and then every hour for the final 2 h, with samples being replaced by fresh,
340 warm HBSS. The same method of transport study was followed as described in the previous
341 section to determine the amount of drug transported during and after the 4h period
342 (Transported) and to evaluate the amount of drug present inside the cells (IN) and remaining
343 on the cells (ON). Additionally, to determine whether drug deposition and transport study
344 altered the epithelial barrier integrity of the Detroit 562 cells, sodium fluorescein permeability
345 assay was conducted on untreated cells that served as control and on treated cells following
346 Lidocaine deposition and post 4 h transport study as described earlier in the previous section.

347

348 **2.15 Statistical analysis**

349 All results are expressed as mean ± standard error of the mean (SEM) of at least three biological
350 replicates. Statistical software, GraphPad Prism (version 8.2.1) was used to test for significance
351 using One-Way or Two-Way ANOVA for each experiment. Significance was determined as p
352 < 0.05.

353 **3. RESULTS AND DISCUSSION**

354 **3.1 Tight junction formation on day 18 of the ALI culture period**

355 To predict the time for functional tight junctions to develop in the ALI for Detroit 562 cell line
356 and determine the optimum seeding density, TEER measurements and permeability of the
357 known paracellular marker flu-Na were tested on days 7, 14, 18 and 21 of the ALI culture
358 periods for all 3 densities (30,000 c/w, 60,000 c/w and 80,000 c/w). TEER values significantly

359 increased from day 7 to 18 with no significant changes in TEER values between day 18 and 21
360 for all the 3 densities, thus indicating progressive tight junction formation till day 18 of the ALI
361 culture period (Figure 2A). Correspondingly, a significant decrease in apparent permeability
362 (P_{app}) of flu-Na was observed on day 18 compared to day 7 and 14 for 60,000 c/w and 80,000
363 c/w ALI models and plateaued till day 21, but not for 30,000 c/w (Figure 2B). These results
364 suggest that the cell layers have developed functional tight junctions in ALI culture at day 18
365 for 60,000 c/w and 80,000 c/w ALI models. Therefore, these two densities, termed Low and
366 High density, respectively, were used for the subsequent experiments as 30,000 c/w ALI
367 models would require a longer time to develop tight junctions and attain epithelial barrier
368 integrity and an extended culture period may induce greater cell death.

369
370

371 **3.2 Abundance of live cells on day 18 of the ALI culture period**

372 A cell viability assay was performed to verify cell survival over the 18 days ALI culture period
373 as extended culture periods can induce cell death and compromise the integrity of cellular
374 barrier properties [23]. The cells cultured in ALI conditions were stained with calcein AM and
375 EthD-1 to determine the live and dead cells, respectively (Figure 3). The fluorescent
376 micrographs show live cells (green), dead cells (red), and nuclei (blue). Calcein AM dye only
377 penetrates through the cellular boundaries of the live cells, staining them as green thus
378 indicating intact cellular membranes, while EthD-1 stains the cells that have lost their
379 membrane integrity as red, indicating the presence of dead cells. Detroit 562 cells seeded at
380 Low density showed an abundance of live cells on day 7 (Figure 3A) that was found to be like
381 day 18 ALI cultures (Figure 3B). Similar results were observed for High-density ALI cultures
382 (Figure 3C-D), suggesting that the cells are viable following 18 days of ALI culture and can be
383 used for experimentation up until 18 days of ALI culture for both densities. However, the

384 number of dead cells observed on day 18 for low density (Figure 2B) is notably lower compared
385 to High density (Figure 3D), suggesting the feasibility of the use of Low-density ALI cultures.

386
387

388 **3.3 Mucus production increases throughout 18 days of the ALI culture period**

389

390 To determine the extent of differentiation of the Detroit 562 cell line over the 18-day culture
391 period in ALI, mucus production was assessed. Alcian blue was used as a marker of mucus
392 production as it stains the glycoproteins present in mucus, producing a blue colour. Mucus
393 production significantly increased for both the densities of the Detroit 562 cell line (Figure 4)
394 during the 18 days ALI culture period, suggesting continued differentiation throughout this
395 period. Day 1 Alcian blue staining of ALI models of the Detroit 562 cell lines showed
396 indistinct, weak blue staining in the micrographs for both Low and High density (Figure 4A-
397 B). Comparatively, the Alcian blue staining increased with greater blue intensity observed in
398 distinct patches on day 18 for both the densities (Figure 4C-D), suggesting the cells continued
399 differentiation till 18 days of the ALI culture period for Detroit 562 cells. Therefore, the
400 increase in mucus production following 18 days of ALI indicates that the Detroit 562 cell line
401 has a mucus-secreting phenotype that continues to differentiate till day 18 of the ALI culture
402 period. These results are in accordance with previous reports [11, 24].

403

404 **3.4 Significant IL-8 production by the Detroit 562 cells in response to LPS and Poly**

405 **(I:C)**

406 To determine whether the ALI model of the Detroit 562 cell line could be used to study
407 responses to bacterial and viral infection, as the throat is often the primary site for these kinds
408 of infections, the Detroit 562 cells on day 18 of the ALI culture period were stimulated with
409 the bacterial endotoxin lipopolysaccharide to mimic bacterial infection [25] and the viral
410 component Poly (I:C) to simulate viral infection [13]. No significant increase in IL-6 and IL-

411 1β production (data not shown) compared to control (unstimulated cells) was observed in the
412 ALI models for both Low and High density. On the contrary, a significant increase in IL-8
413 production was observed in the LPS-stimulated cells post 24 and 48 h of stimulation (Figure
414 5A) compared to control ($p < 0.0001$ respectively) for both low- and high-density ALI models,
415 suggesting that these models could be used to mimic bacterial infection. As no significant
416 differences in IL-8 production were observed between 24 and 48 h of LPS stimulation for both
417 densities (Figure 5A), 24 h of LPS stimulation can be considered sufficient to model bacterial
418 infection for these ALI models.

419 Like the IL-8 cytokine secretion profile of LPS-stimulated Detroit 562 cells (Figure 5A), IL-8
420 production by the Poly: IC stimulated Detroit 562 cells following the same pattern (Figure 5B).
421 Poly (I:C)-mediated IL-8 secretion was significantly increased at both low and high densities
422 of the Detroit 562 cell line post 24 and 48 hrs of stimulation (Figure 5B). Comparable
423 concentrations were observed between the two densities at both time points, agreeing with
424 previously published reports [26, 27], reinforcing the finding that the ALI model could be used
425 to model viral infection post 24 hrs of Poly (I:C) stimulation. Additionally, no significant
426 changes in the TEER measurements (Figure 5C) and P_{app} values (Figure 5D) of the LPS and
427 Poly (I:C) stimulated cells were found compared to the control for both the densities, thus
428 indicating that the epithelial barrier integrity of the Detroit 562 cells was maintained post-
429 stimulation. These results further confirm the suitability of the day 18 Detroit 562 ALI model
430 to simulate both bacterial and viral infection.

431

432 **3.5 Confirmation of tight junction formation**

433 To corroborate the development of tight junctions of the ALI models on day 18 for the Detroit
434 562 cell line, the ALI models were visualized by immunolabelling the cells with markers of
435 tight junction proteins Zona Occludens (ZO-1) over the 18 days of ALI culture period. Z-
436 projections of the confocal micrographs show ZO-1 (green), and nuclei (blue) and the merged

437 images are presented in Figure 5A-B. Punctate formation of ZO-1 positive tight junctions was
438 only visible on day 18 of the ALI culture period (data not shown for other days 7 and 14)
439 (Figure 6A-B). ZO-1 positive tight junctions were observed along cell-cell contacts throughout
440 the cellular layers for both the Low and High density of the Detroit 562 cell line (Figure 6A-
441 B, shown by the white arrows), similar to previously published results [28]. Overall, the
442 visualization of the tight junction formation of the day 18 Detroit 562 ALI cultures for both
443 densities (Figure 6A-B) corroborates the earlier findings of the significant increase in TEER
444 measurements of these ALI models on day 18 compared to day 7 (Figure 2A) and the
445 corresponding decrease in P_{app} of the paracellular marker (Figure 2B). Taken together, these
446 results suggest complete differentiation of the Detroit 562 cell line at day 18 of the ALI culture
447 period and attainment of epithelial barrier integrity, irrespective of the seeding densities used
448 and fitness of these *in vitro* models to investigate drug transport.

449

450 **3.6 Lidocaine transport across the Detroit 562 ALI models**

451

452 A transport study was conducted to determine if the differentiated ALI models of Detroit 562
453 cells could be used to study drug transport, using Lidocaine as a model drug on day 18 post
454 ALI. Lidocaine solution (20 $\mu\text{g}/\text{mL}$) was added to the apical surface and basal samples were
455 collected and analysed to confirm Lidocaine transport over 4 hours. The cumulative mass of
456 Lidocaine in the basal samples increased with time for both low- and high-density ALI cultures
457 (Figure 7A) with no significant differences, suggesting that Lidocaine had been transported
458 through both the ALI cultures. Notably, no Lidocaine was found inside the cells (shown as
459 Cellular, Figure. 7B), suggesting that Lidocaine may have been transported using the
460 paracellular pathway.

461 Seeding density is a key factor that influences the formation of tight junctions and higher
462 densities may negatively impact the transport of certain drugs [29]. The percentage of the total

463 mass of Lidocaine transported after 4 hours across the low- and high-density ALI cultures were
464 not significantly different (Low: 47.3 ± 2.36 %, High: 47.53 ± 1.67 %) (Figure 6B), thus
465 indicating the suitability of the Low-density ALI culture of Detroit 562 cell line as an *in vitro*
466 model of drug transport. Furthermore, no significant changes in TEER values (Figure 7C) and
467 apparent permeability (P_{app}) values (Figure 7D) were observed between pre and post Lidocaine
468 transport study for both densities, confirming that Lidocaine deposition and transport did not
469 alter the epithelial barrier integrity of both low- and high-density ALI cultures.

470 Comparative analysis of the apparent permeability (P_{app}) of flu-Na and Lidocaine in the ALI
471 cultures on day 18 showed that Lidocaine was transported at a significantly higher rate than
472 the flu-Na molecule for both low- and high-density ALI cultures ($p < 0.0001$ respectively,
473 Figure 7E). The significantly increased transport of Lidocaine cannot be attributed to charge as
474 both the Lidocaine and flu-Na molecules are negatively charged. Thus, the increased
475 permeability of Lidocaine may be due to the difference in the molecular weight of the two
476 molecules, with a significantly greater number of the Lidocaine molecules (MW 234.3 g/mol)
477 able to permeate via the tight junctions compared to flu-Na (MW 376.3 g/mol). Overall, the
478 results suggest the involvement of the paracellular pathway in the transport of Lidocaine across
479 the Detroit 562 ALI cultures, but this needs to be further explored.

480 Altogether, the study indicates that the Detroit 562 cell line completely differentiates at day 18
481 in ALI and the suitability of the low-density ALI culture ($60,000$ cells/well or 1.8×10^5
482 cells/cm²) as a representative *in vitro* air-liquid interface cellular model to study drug transport
483 on day 18 of the ALI culture period.

484

485

486 **3.7 Optimisation of the experimental parameters for the novel 3-D printed throat model**

487

488 The experimental parameters (specifically the flow rate and angle at which the Lidocaine throat
489 spray was positioned for each shot) required to study drug deposition in the throat region were
490 determined using the currently used USP-IP throat model. Lidocaine deposition was detected
491 in the mouthpiece, throat, and Stage 1 (shown as S1, Figure 8A-B) for all the 3 flow rates (0,
492 15 and 30 L/min) at both 45° (Figure 8A) and 90° (Figure 8B) but was not found in the lower
493 stages of the NGI (Stages 2-7, data not shown). No significant differences in mass of drug
494 deposited in the throat region were observed between the three flow rates (0, 15, 30 L/min) at
495 45° angle (shown as Throat, Figure 8A) and at 90° angle (Figure 8B). Therefore, a flow rate of
496 30 L/min was chosen as the optimum flow rate for subsequent studies as it represents normal
497 breathing conditions. Furthermore, since there were no significant differences in the Lidocaine
498 mass deposited in the throat region between the two angles - 45° and 90° at the optimised flow
499 rate of 30 L/min (Table 1), the 45° angle was chosen for the subsequent experiments as it
500 represents the position at which the throat spray is usually held by the users.

501 Lidocaine deposition studies were then performed using the physiologically representative 3D-
502 printed throat model at the optimised flow rate of 30 L/min and an angle of 45°. The results
503 showed a significant increase in Lidocaine deposition in the throat region of the 3D-printed
504 throat model in comparison to the mouthpiece and Stage 1 (Figure 9), with no drug detected in
505 the lower stages of the NGI (Stages 2-7, data not shown), thus showing the suitability of the
506 throat model to study drug deposition. A comparison of Lidocaine deposition between the USP-
507 IP throat model and the developed 3-D printed VCU model further showed no significant
508 differences in drug deposition between the two throat models (Table 2). Overall, these results
509 show that the developed 3D-printed throat model could be used to study Lidocaine deposition
510 at a flow rate of 30 L/min and an angle of 45°.

511

3.7 Transport study of Lidocaine using the novel 3-D printed throat model integrated with an *in vitro* cellular model

Before conducting the transport study, the number of shots delivered from the Lidocaine throat spray to the cells incorporated within the 3-D throat model required to achieve a suitable amount that would be above the limit of analytical detection was optimised using empty snapwell inserts. The optimization of the number of shots was also performed as a greater number of shots may change the epithelial barrier integrity of the cells, compromising the cell viability. The experiment was performed using 1 and 3 shots of Lidocaine spray at a flow rate of 30 L/min, at an angle of 45° (Figure 10A). The number of shots chosen to perform the transport study was 1 shot as it is likely to have less impact on the cellular layers of the Detroit 562 ALI model in comparison to 3 shots and thus will enable the cells to retain their epithelial barrier integrity after drug deposition and during the 4h transport study.

Next, the completely differentiated *in vitro* ALI cultures of Detroit 562 cells grown on snapwells were placed inside the 3D-printed throat model (one Snapwell in the upper position referred to as Upper and the other snapwell in the lower position referred to as Lower). Then, one shot of Lidocaine spray was fired onto the throat model at a flow rate of 30 L/min⁻¹ using an angle of 45° to study drug transport across the developed *in vitro* throat model integrated with the cellular model. The cumulative mass of Lidocaine transported across the cellular layers of the Detroit 562 ALI cultures significantly increased with time for Upper Snapwell (shown as white circles, Figure 10B) from 0.5 h till 2 h ($p < 0.001$, Figure 10B) and then plateaued till 4 h (Figure 10B), suggesting that Lidocaine was transported across the ALI cultures. Comparatively, no significant differences were observed for the cumulative mass of Lidocaine transported for the Lower Snapwell (shown as black circles, Figure 10B) between 0.5 hours and 2 hours and the remaining of the transport study. Furthermore, the mass of

537 Lidocaine transported after 4 hours in the Upper Snapwell ($76.5 \pm 5.7 \mu\text{g}$) was significantly
538 higher compared to the Lower Snapwell ($8.24 \mu\text{g} \pm 6.45 \mu\text{g}$). This data correlates with the
539 results of the optimisation experiment for the number of shots that showed significantly
540 decreased Lidocaine deposition for the Lower Snapwell compared to the Upper Snapwell
541 (Figure 10A) indicating that the position of the Snapwells affects drug deposition and transport.

542 Importantly, a significantly higher percentage of Lidocaine was transported in case of the
543 aerosol spray at a significantly greater rate (Figure 9C-D) compared to the Lidocaine drug
544 solution (Figure 7B-E) at the end of the 4 hours transport study. These results show higher drug
545 transport of the aerosol spray compared to the drug solution using the 3-D printed throat model,
546 thus highlighting the feasibility of the developed novel 3D-printed throat model to study drug
547 transport using Lidocaine aerosol spray. Furthermore, a significantly lower percentage of drug
548 was found inside the cells compared to the percentage of drug transported (Figure 9C),
549 corroborating with the findings of the transport study of Lidocaine solution (Figure 7B),
550 suggesting that Lidocaine may have followed the paracellular pathway. However, the primary
551 route of transport for Lidocaine remains unclear and needs to be further investigated.

552 To determine whether Lidocaine drug deposition and 4 hours of transport study altered the
553 epithelial barrier integrity of the Detroit 562 ALI culture, a sodium fluorescein permeability
554 assay was performed on the ALI cultures post transport and compared to untreated cells
555 (control). No significant differences in apparent permeability of Flu-Na (P_{app}) were found
556 between the Lower Snapwell and the control (Figure 10D), suggesting that drug deposition did
557 not affect the epithelial barrier integrity of the cells in the Lower Snapwell. However, a
558 significantly higher flu-Na P_{app} value was observed for the Upper Snapwell in comparison to
559 control (untreated cells) ($p < 0.01$, Figure 10D). This could be due to significantly higher drug
560 deposition in the Upper Snapwell that led to the opening up of the tight junctions by Lidocaine,
561 thus increasing Flu-Na permeability and in turn paracellular flux as reported in a recent study

562 [30]. Overall, the study showed that the novel 3D-printed throat model incorporating the *in*
563 *vitro* cellular model could be used to investigate drug transport of therapies targeted at the
564 throat region.

565 566 **4. CONCLUSION**

567
568 The present study indicated the suitability of the novel 3D printed throat model incorporating
569 Detroit 562 cells grown in the ALI configuration as a representative *in vitro* throat model to
570 investigate drug transport of therapies targeted at the oro-pharyngeal region. This study has
571 shown that the Detroit 562 cells completely differentiate on day 18 of ALI at an optimised
572 density of 60,000 cells/well (1.8×10^5 cells/cm²) with significant mucus production, showing
573 response in IL-8 production to LPS and Poly (I:C) stimulus and development of functional tight
574 junctions. Importantly, the developed cell integrated throat model showed Lidocaine transport,
575 possibly via the paracellular pathway, suggesting the suitability of the novel *in vitro* model to
576 study drug transport. Overall, the study highlights the potential of the novel 3-D printed throat
577 model integrated with the optimised cellular model of the Detroit 562 cell line as a promising
578 *in vitro* model to investigate the transport of inhaled drug therapies and predict the therapeutic
579 efficacy of drug-aerosol particles targeting the throat region. Future studies may involve an
580 extension of the current setup towards a complex co-culture system of primary epithelial cells
581 of throat origin for an enhanced *in vitro-in vivo* correlation.

582 **ETHICAL STATEMENTS**

583
584 **Ethics Approval and consent to participate:**

585
586 Not applicable

587
588 **Consent for Publication:**

589
590 Not applicable

591
592

593 **Availability of Data and Materials:**

594 The datasets generated during and/or analysed during the current study are available from the
595 corresponding author on reasonable request.

596 **Competing interests:**

597 The authors have no relevant financial or non-financial interests to disclose.

598 **Funding:**

599
600 The authors declare that no funds, grants or other support were received during the preparation
601 of this manuscript.

602 **Author Contributions:**

603
604 **Zara Sheikh:** Conceptualization, Methodology, Investigation, Data curation, Formal analysis,
605 Writing – original draft, Writing – review & editing, Visualization. **Antonella**
606 **Granata:** Methodology, Investigation, Visualization, Data curation, Formal analysis, Writing
607 - review & editing, Writing - original draft. **Ye Zhang:** Investigation, Data curation, Formal
608 analysis. **Hanieh Mohammad Gholizadeh Mahvizani:** Visualization, Investigation, Formal
609 analysis. **Dina Silva:** Conceptualization, Methodology. **Paul M. Young:** Conceptualization,
610 Resources. **Luca Casettari:** Conceptualization, Methodology, Validation, Writing - review &
611 editing. **Hui Xin Ong:** Conceptualization, Methodology, Validation, Writing - review &
612 editing, Writing - original draft, Resources, Supervision. **Daniela Traini:** Conceptualization,
613 Methodology, Writing - review & editing, Writing - original draft, Validation, Resources,
614 Supervision.

615 **Acknowledgments:**

616 The authors would like to thank Dr Jesse Xu for his technical support in 3D printing of the
617 throat model.

618

619 **Conflicts of Interest Disclosure:**

620 All authors declare that they have no conflict of interests.

621 **REFERENCES**

622

623 [1] S. Hasan, P. Sebo, R. Osicka, A guide to polarized airway epithelial models for studies of host–
624 pathogen interactions, *The FEBS Journal*, 285 (2018) 4343-4358.

625 [2] S. van Riet, D.K. Ninaber, H.M.M. Mikkers, T.D. Tetley, C.R. Jost, A.A. Mulder, T. Pasman, D. Baptista,
626 A.A. Poot, R. Truckenmüller, C.L. Mummery, C. Freund, R.J. Rottier, P.S. Hiemstra, In vitro modelling
627 of alveolar repair at the air-liquid interface using alveolar epithelial cells derived from human induced
628 pluripotent stem cells, *Scientific Reports*, 10 (2020) 5499.

629 [3] B. Forbes, C. Ehrhardt, Human respiratory epithelial cell culture for drug delivery applications,
630 *European journal of pharmaceuticals and biopharmaceutics : official journal of Arbeitsgemeinschaft fur*
631 *Pharmazeutische Verfahrenstechnik e.V.*, 60 (2005) 193-205.

632 [4] Z. Sheikh, P. Bradbury, M. Pozzoli, P.M. Young, H.X. Ong, D. Traini, An in vitro model for assessing
633 drug transport in cystic fibrosis treatment: Characterisation of the CuFi-1 cell line, *European journal*
634 *of pharmaceuticals and biopharmaceutics : official journal of Arbeitsgemeinschaft fur Pharmazeutische*
635 *Verfahrenstechnik e.V.*, 156 (2020) 121-130.

636 [5] H.X. Ong, D. Traini, M. Bebawy, P.M. Young, Ciprofloxacin is actively transported across bronchial
637 lung epithelial cells using a Calu-3 air interface cell model, *Antimicrobial agents and chemotherapy*, 57
638 (2013) 2535-2540.

639 [6] A.E. Luengen, C. Kniebs, E.M. Buhl, C.G. Cornelissen, T. Schmitz-Rode, S. Jockenhoevel, A.L. Thiebes,
640 Choosing the Right Differentiation Medium to Develop Mucociliary Phenotype of Primary Nasal
641 Epithelial Cells In Vitro, *Scientific Reports*, 10 (2020) 6963.

642 [7] M.A. Selo, J.A. Sake, K.-J. Kim, C. Ehrhardt, In vitro and ex vivo models in inhalation
643 biopharmaceutical research — advances, challenges and future perspectives, *Advanced Drug Delivery*
644 *Reviews*, (2021) 113862.

645 [8] O.H. Wittekindt, Tight junctions in pulmonary epithelia during lung inflammation, *Pflugers Archiv :*
646 *European journal of physiology*, 469 (2017) 135-147.

647 [9] J. Zhou, X.-d. Zhou, R. Xu, X.-z. Du, Q. Li, B. Li, G.-y. Zhang, L.-x. Chen, J.M. Perelman, V.P. Kolosov,
648 The Degradation of Airway Epithelial Tight Junctions in Asthma Under High Airway Pressure Is Probably
649 Mediated by Piezo-1, *Frontiers in Physiology*, 12 (2021).

650 [10] S.N. Georas, F. Rezaee, Epithelial barrier function: at the front line of asthma immunology and
651 allergic airway inflammation, *The Journal of allergy and clinical immunology*, 134 (2014) 509-520.

652 [11] C.M. Weight, C. Venturini, S. Pojar, S.P. Jochems, J. Reiné, E. Nikolaou, C. Solórzano, M.
653 Noursadeghi, J.S. Brown, D.M. Ferreira, R.S. Heyderman, Microinvasion by *Streptococcus pneumoniae*
654 induces epithelial innate immunity during colonisation at the human mucosal surface, *Nature*
655 *Communications*, 10 (2019) 3060.

656 [12] P.A. Ryan, V. Pancholi, V.A. Fischetti, Group A streptococci bind to mucin and human pharyngeal
657 cells through sialic acid-containing receptors, *Infect Immun*, 69 (2001) 7402-7412.

658 [13] L. Tengroth, C.R. Millrud, A.M. Kvarnhammar, S. Kumlien Georén, L. Latif, L.-O. Cardell, Functional
659 effects of Toll-like receptor (TLR)3, 7, 9, RIG-I and MDA-5 stimulation in nasal epithelial cells, *PLoS One*,
660 9 (2014) e98239-e98239.

661 [14] A. Kaviratna, G. Tian, X. Liu, R. Delvadia, S. Lee, C. Guo, Evaluation of Bio-relevant Mouth-Throat
662 Models for Characterization of Metered Dose Inhalers, *AAPS PharmSciTech*, 20 (2019) 130.

663 [15] Y. Zhang, K. Gilbertson, W.H. Finlay, In vivo-in vitro comparison of deposition in three mouth-
664 throat models with Qvar and Turbuhaler inhalers, *Journal of aerosol medicine : the official journal of*
665 *the International Society for Aerosols in Medicine*, 20 (2007) 227-235.

666 [16] B. Olsson, L. Borgström, H. Lundbäck, M. Svensson, Validation of a general in vitro approach for
667 prediction of total lung deposition in healthy adults for pharmaceutical inhalation products, *J Aerosol*
668 *Med Pulm Drug Deliv*, 26 (2013) 355-369.

669 [17] C.A. Ruzycski, L. Golshahi, R. Vehring, W.H. Finlay, Comparison of in vitro deposition of
670 pharmaceutical aerosols in an idealized child throat with in vivo deposition in the upper respiratory
671 tract of children, *Pharmaceutical research*, 31 (2014) 1525-1535.

672 [18] J.G. Weers, A.R. Clark, N. Rao, K. Ung, A. Haynes, S.K. Khindri, S.A. Perry, S. Machineni, P.
673 Colthorpe, In Vitro-In Vivo Correlations Observed With Indacaterol-Based Formulations Delivered with
674 the Breezhaler®, *J Aerosol Med Pulm Drug Deliv*, 28 (2015) 268-280.

675 [19] R.R. Delvadia, P.W. Longest, P.R. Byron, In vitro tests for aerosol deposition. I: Scaling a physical
676 model of the upper airways to predict drug deposition variation in normal humans, *J Aerosol Med
677 Pulm Drug Deliv*, 25 (2012) 32-40.

678 [20] R. Delvadia, M. Hindle, P.W. Longest, P.R. Byron, In vitro tests for aerosol deposition II: IVIVCs for
679 different dry powder inhalers in normal adults, *J Aerosol Med Pulm Drug Deliv*, 26 (2013) 138-144.

680 [21] X. Wei, M. Hindle, R.R. Delvadia, P.R. Byron, In Vitro Tests for Aerosol Deposition. V: Using Realistic
681 Testing to Estimate Variations in Aerosol Properties at the Trachea, *J Aerosol Med Pulm Drug Deliv*, 30
682 (2017) 339-348.

683 [22] C.M. Weight, C. Venturini, S. Pojar, S.P. Jochems, J. Reiné, E. Nikolaou, C. Solórzano, M.
684 Noursadeghi, J.S. Brown, D.M. Ferreira, R.S. Heyderman, Microinvasion by *Streptococcus pneumoniae*
685 induces epithelial innate immunity during colonisation at the human mucosal surface, *Nat Commun*,
686 10 (2019) 3060.

687 [23] A. Hassanzadeh-Barforoushi, A.M.K. Law, A. Hejri, M. Asadnia, C.J. Ormandy, D. Gallego-Ortega,
688 M. Ebrahimi Warkiani, Static droplet array for culturing single live adherent cells in an isolated
689 chemical microenvironment, *Lab on a chip*, 18 (2018) 2156-2166.

690 [24] P.A. Ryan, V. Pancholi, V.A. Fischetti, Group A streptococci bind to mucin and human pharyngeal
691 cells through sialic acid-containing receptors, *Infect Immun*, 69 (2001) 7402-7412.

692 [25] L. Borghini, M. Hibberd, S. Davila, Changes in H3K27ac following lipopolysaccharide stimulation
693 of nasopharyngeal epithelial cells, *BMC Genomics*, 19 (2018) 969.

694 [26] L. Tengroth, C.R. Millrud, A.M. Kvarnhammar, S. Kumlien Georén, L. Latif, L.O. Cardell, Functional
695 effects of Toll-like receptor (TLR)3, 7, 9, RIG-I and MDA-5 stimulation in nasal epithelial cells, *PLoS One*,
696 9 (2014) e98239.

697 [27] C. Rydberg, A. Månsson, R. Uddman, K. Riesbeck, L.O. Cardell, Toll-like receptor agonists induce
698 inflammation and cell death in a model of head and neck squamous cell carcinomas, *Immunology*, 128
699 (2009) e600-611.

700 [28] T. Sumitomo, M. Nakata, M. Higashino, M. Yamaguchi, S. Kawabata, Group A *Streptococcus*
701 exploits human plasminogen for bacterial translocation across epithelial barrier via tricellular tight
702 junctions, *Scientific Reports*, 6 (2016) 20069.

703 [29] G.C. Williams, G.T. Knipp, P.J. Sinko, The Effect of Cell Culture Conditions on Saquinavir Transport
704 Through, and Interactions with, MDCKII Cells Overexpressing hMDR1, *Journal of Pharmaceutical
705 Sciences*, 92 (2003) 1957-1967.

706 [30] A.R. Santa-Maria, F.R. Walter, S. Valkai, A.R. Brás, M. Mészáros, A. Kincses, A. Klepe, D. Gaspar,
707 M.A.R.B. Castanho, L. Zimányi, A. Dér, M.A. Deli, Lidocaine turns the surface charge of biological
708 membranes more positive and changes the permeability of blood-brain barrier culture models,
709 *Biochimica et Biophysica Acta (BBA) - Biomembranes*, 1861 (2019) 1579-1591.

710

711

712 **LIST OF TABLES**

713

714

715 **Table 1.** Comparison of Lidocaine mass deposition in the USP-IP throat region using the
716 simulated respiratory tract (Next-Generation Impactor (NGI) between 45° and 90° angles at

717 optimised flow rate of 30 L/min. (N=3, mean \pm SEM) ns = no significance (using one-way
 718 ANOVA with Tukeys post test)

719

720

Flow rate (L/min)	Mass deposited (mg) at 45°	Mass deposited (mg) at 90°	Statistical Analysis
30	20.9 \pm 0.7	17.9 \pm 0.5	ns

721

722

723 **Table 2.** Comparison of Lidocaine mass deposition in the throat region between USP-IP throat
 724 model and the developed 3-D printed VCU throat model at optimised flow rate of 30 L/min
 725 and 45°. (N=3, mean \pm SEM) ns = no significance (using one-way ANOVA with Tukeys post
 726 test)

	USP-IP model	3D Throat model	Statistical Analysis
Mass deposited (mg)	21 \pm 1.3	23 \pm 3.9	ns

727

728

729

730

731 **FIGURE LEGENDS**

732 **Fig. 1 A** Developed modified 3D printed throat model **B** Lower Snapwell (snapwell insert
 733 placed at the bottom position shown with black arrow) **C** Upper Snapwell (snapwell insert
 734 placed at the top position shown with black arrow)

735 **Fig. 2** Air-liquid interface (ALI) culture model of Detroit 562 cell line over a culture period of
 736 21 days for all 3 densities (30,000 c/w, 60,000 c/w and 80,000 c/w). **A** Transepithelial electrical

737 resistance measurements (TEER) and **B** Apparent permeability (Papp) of sodium fluorescein
738 (flu-Na) across Detroit 562 ALI cultures (n=3, mean ± SEM) * p < 0.05, ** p < 0.01, *** p <
739 0.001, **** p < 0.0001 (using two-way ANOVA with Tukeys post test)

740 **Fig. 3** Live and Dead Images of Detroit 562 ALI cultures at Low density on **A** Day 7 and **B**
741 Day 18 of ALI culture and at High density on **C** Day 7 and **D** Day 18 of ALI culture. Shown
742 are Live cells (green), Dead cells (red), Hoescht (blue) and Merged images. Scale bar: 50 µm.
743 (n = 3, mean ± SEM)

744 **Fig. 4** Mucus production of Detroit 562 ALI cultures on Day 1 of ALI culture period for **A**
745 Low and **B** High density ALI cultures compared to Day 18 for **C** Low and **D** High density ALI
746 cultures (Scale bar = 0.5 mm)

747 **Fig. 5** IL-8 production of Detroit ALI cultures after 24 and 48h of **A** LPS stimulation **B** Poly:IC
748 stimulation **C** Transepithelial electrical resistance measurements (TEER) and **D** Apparent
749 permeability (Papp) of sodium fluorescein (flu-Na) across Detroit 562 ALI cultures post LPS
750 and Poly I:C stimulation (n=3, mean ± SEM) **** p < 0.0001 (using two-way ANOVA with
751 Tukeys post test)

752 **Fig. 6** Tight Junction Formation at Day 18 for **A** Low and **B** High density ALI cultures of
753 Detroit 562 cells. Confocal images A-B represent 3D volume reconstructions (X,Y,Z) of zona
754 occludens (ZO-1) (green), DAPI (blue) and Merged Images. White arrows represents an
755 example of ZO-1 positive tight junction formation throughout the slices (n=3, scale bar = 50
756 um)

757 **Fig. 7** Transport of Lidocaine across ALI models of Detroit 562 cells on Day 18 of ALI culture
758 period for both Low and High densities. **A** Cumulative mass of Lidocaine transported over 4 h
759 period at Low density and High density cells of Detroit 562 ALI models **B** Percentage of the
760 total mass of Lidocaine transported across the ALI cultures (shown as Transported), remaining

761 on the apical layers (On) and inside the cells (Cellular) in Low and High density cells at the
762 end of the experiment (4 h) **C** TEER measurements **D** Flu-Na permeability of ALI cultures
763 before drug deposition (control) and after 4 h of Lidocaine transport (shown as Post transport).
764 **E** Apparent permeability (Papp) comparison between flu-Na and Lidocaine across ALI cultures
765 (n=3, mean ± SEM) (**** p < 0.0001) using two-way ANOVA with Tukeys post test)

766 **Fig. 8** Lidocaine deposition in the mouthpiece, USP-IP throat and stage 1 (S1) of the simulated
767 respiratory tract (Next-Generation Impactor (NGI) at **A** 45° and **B** 90° angles at 3 different
768 three flow rates (0, 15 and 30 L/min) (N=3, mean ± SEM) ** p < 0.01, *** p < 0.001, **** p
769 < 0.0001 (using two-way ANOVA with Tukeys post test)

770 **Fig. 9** Lidocaine deposition in the mouthpiece, 3-D printed throat model and stage 1 (S1) using
771 the simulated respiratory tract (Next-Generation Impactor (NGI) at the optimised flow rate of
772 30 L/min and 45° angle (N=3, mean ± SEM) **** p < 0.0001 (using one-way ANOVA with
773 Tukeys post test)

774 **Fig. 10** Transport of Lidocaine across throat cell integrated 3-D printed throat model **A**
775 Optimization of number of shots of Lidocaine spray for transport experiment **B** Cumulative
776 mass of Lidocaine transported over 4 h period across cellular layers of Detroit 562 ALI models
777 for Lower and Higher Snapwells **C** Percentage of the total mass of Lidocaine transported
778 across the ALI cultures (shown as Transported), remaining on the apical layers (On) and inside
779 the cells (Cellular) of the Lower and Higher Snapwells at the end of the experiment (4 h) **D**
780 Flu-Na permeability of ALI cultures before drug deposition (control) and post 4 h of Lidocaine
781 transport (n=3, mean ± SEM) (* p < 0.05, ** p < 0.01, **** p < 0.0001)

782

783